S. DURGA BHAVANI,[1,2] K. VIJAYA KUMAR,[3] B. PURNA CHANDRA RAO,[2]
CH. SHILPA CHAKRA,[4] KIRAN KUMAR GANTA[5]

[1] Department of Chemistry, Government Degree College Rajendranagar
(Rangareddy-District – 501218, Telangana, India)
[2] Department of Chemistry, Gandhi Institute of Technology and Management
(Hyderabad-502 329, Telangana, India)
[3] Department of Physics, JNTUH University College of Engineering Jagtial
(Nachupally (Kondagattu), Jagtial-District – 505501, Telangana, India;
e-mail: kvkphd@gmail.com)
[4] Centre for Nano Science and Technology,
JNTUH University College of Engineering Science and Technology Hyderabad
(Telangana, India)
[5] Department of Physics, B V Raju Institute of Technology
(Narsapur, Medak-District, 502313, Telangana, India)

A STUDY OF THE FINE-TUNING OF THE OPTICAL ENERGY BAND GAP AND VARIOUS OPTICAL PARAMETERS WITH THE IMPACT OF GADOLINIUM COMPOSITION IN NGFO FERRITE NANOPARTICLES

UDC 539

In the present work, gadolinium-doped nickel ferrite nanoparticles with the chemical composition $NiFe_{2-x}Gd_xO_4$ ($X = 0.00, 0.05, 0.10, 0.15, 0.20$, and 0.25) have been prepared by the sol-gel auto-combustion method and calcinated at 700 °C. The spinel ferrite phase formation was confirmed with the XRD graphs. In all the samples, the typical absorbance peak was observed in between 250–300 nm. Tauc plots were used to calculate the optical energy band gap, found in the range of 4.033–4.144 eV, and it was also calculated using x-ray density to be in the range of 3.690–4.300 eV. Both of them were observed in good agreement with each other, and we conclude that the Gd composition could finely tune the optical energy band gap. The impact of Gd composition was clearly observed on optical parameters. The refractive index, reflectivity, absorption coefficient, optical dielectric constant, and dielectric susceptibility have shown the increasing tendency from 2.1140 to 2.2325, 12.80 to 14.53%, 5.4380 to 6.3032 cm^{-1}, 3.4690 to 3.9840 and 0.2760 to 0.3170, respectively, whereas the transmission coefficient decreased from 0.7730 to 0.7461.

Keywords: NGFO nanoparticles, optical energy band gap, refractive index, absorption coefficient, optical dielectric constant.

1. Introduction

Among all the ferrites, the spinel ferrites are most promising magnetic oxides with their excellency in magnetic, dielectric, and optical properties. An extensive research has been carried out in the vicinity of magnetic and dielectric properties, whereas the focus on their optical properties was not found much. Accordingly, if we identify the history of ferrites back to the 1950s, the industry flourished due to the widespread use of ferrite cores in television sets and the high demand for television sets globally. The researchers' attention was later redirected

Citation: Bhavani S. Durga, Kumar K. Vijaya, Rao B. Purna Chandra, Chakra Ch. Shilpa, Ganta Kiran Kumar. A study on fine-tuning the optical energy band gap and various optical parameters with the impact of gadolinium composition in NGFO ferrite nanoparticles. *Ukr. J. Phys.* **69**, No. 5, 304 (2024). https://doi.org/10.15407/ ujpe69.5.304.
Цитування: Бхавані С. Дурга, Кумар К. Віджая, Рао Б. Пурна Чадра, Чакра Ч. Шілпа, Ганта Кіран Кумар. Дослідження тонкого налаштування оптичної забороненої зони і різних оптичних параметрів зміною вмісту гадолінію в NGFO феритових наночастинках. *Укр. фіз. журн.* **69**, № 5, 304 (2024).

from bulk ferrites to nanoferrites. While comparing the behavior of ferrites in nanoform to their bulk form, which was synthesized using different methods, significant differences were observed [1]. Due to the widespread use of opto-electronic devices like radios, video tape recorders, TVs, and internet technology by large segments of society worldwide, the market situation has changed, which has raised demand for both bulk and nanoferrites. The first commercial soft ferrite was used as an inductor in LC-filters which were used in the frequency division multiplex equipment [2]. Those filters needed to have a potent dielectric and effective magnetic properties, because they operated in the 50–450 kHz frequency range. The advanced technologies of today have demanded nanoferrites with special optical characteristics. The human race may finally be equipped with innovative and superior nanoferrite-based devices, which would connect not only their optical properties, but also their core magnetic, magneto-electric, and multiferroic behavior. In such circumstances, the study of optical properties of nanoferrites has gained importance. However, because of the notable differences between the physical and chemical characteristics of $NiFe_2O_4$ nanoparticles in comparison to those of free atoms or molecules, as well as their counter bulk solids, some researchers have focused their attention toward these particles due to their extensive range of potential applications which include high-frequency, the cores of radiofrequency transformers, inductors, antennas, and materials that absorb radar emission. They also belong to the soft magnetic material family and have low coercivity, high electric resistivity, moderate magnetic saturation, and low hysteresis losses [3–4]. In addition, they have plenty of potential for degradation of both inorganic and organic pollutants as catalysts and/or catalytic supports. By means of their unique combination of magnetic properties, antimicrobial activity, and thermal treatment of cancer, $NiFe_2O_4$ nanoparticles are becoming increasingly significant in biomedical applications like systems for delivering medications, hyperthermia therapies for cancer, and magnetic resonance imaging (MRI) [5–6]. Moreover, doping and synthesis techniques are essential for improving their physical and chemical characteristics, which are critical for uses such as industrial applications, photocatalysis, and electrochemical energy storage materials [7–8]. Further, the doping of rare-earth elements becomes of importance due to their outstanding performance. In the case of rare earth metals (La^{3+}, Ce^{3+}, Pr^{3+}, Gd^{3+}, Dy^{3+}, and Ho^{3+}) strong spin-orbit coupling of unpaired 4f electrons that are isolated by "5s" and "5p" shells are the causes of magnetism and their magnetic moments are thus included within the atomic system. Thus, the substitution of rare earth ions into the spinel ferrite structure can result in 3d–4f coupling, which may signi ficantly modify the properties of the material [9–10]. Among the lanthanide group, gadolinium (Gd^{3+}) has '$4f^7$' valence electrons, and its magneto crystalline anisotropy [11], the doping of ferrites with Gd^{3+} ions can produce a material that can be effectively utilized in microwave devices, magnetic storage, and recording devices [12]. The literature review suggests that, in order to fulfil the requirements of the technological sector, fascinating variations in spinel ferrites can be achieved by incorporating rare-earth cations [13–14]. Further, doped ferrites are used to improve photocatalytic efficiency, magnetic separability, visible light absorption, and other optical applications in addition to electrical-magnetic applications. [15]. Two fundamental properties, the optical energy band gap and the refractive index, would determine the optical and electronic behavior of any given material. Additionally,, among the most significant features that must be studied in order to use a material in these applications are optical dielectric behavior and electronic polarizability; these characteristics are further connected to refraction, electrooptical effect, and optical nonlinearity. [16–17]. Because of their superior optical characteristics, materials with a high refractive index (>2) are important in nonlinear optics. Numerous optical characteristics also exhibit a clear correlation with refractive index. To put it briefly, research is necessary to determine how closely related electrical and optical properties are in order to use a new material for particular purposes. Still, a lot of current research focuses on the structural, magnetic, and electrical characteristics of both pure and doped ferrite nanoparticles [18]. But no reports are available on the impact of Gadolinium composition on optical parameters of NGFO ferrite nanoparticles in in the literature. Therefore, the current communication presents the influence of Gd^{+3} composition on several optical parameters of NGFO ferrite nanoparticles; that are synthesized following the sol-gel autocombustion method and optical parameters are well explained with regard for structural parameters and

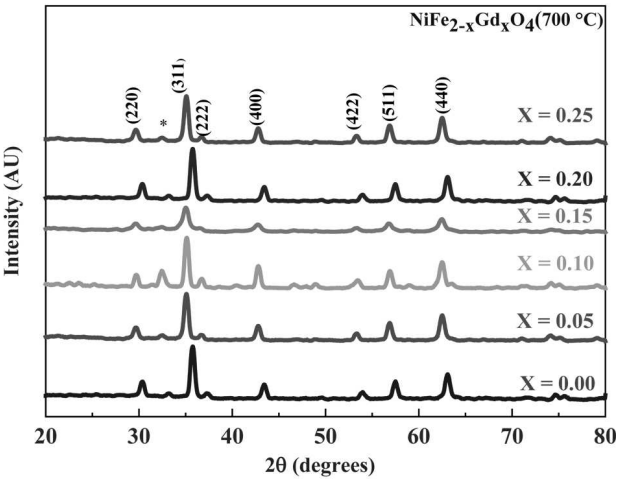

Fig. 1. XRD patterns of $NiFe_{2-x}Gd_xO_4$ ($x = 0.00$, 0.05, 0.10, 0.15, 0.20 0.25) nanoparticles calcinated at 700 °C [K.V. Kumar *et al. Eur. Chem. Bull.* **12** (4), 10479 (2023)]

the optical energy band gap that has been experimentally determined. The results of all these computations can give a precise recipe for creating composites for the use in optical and optoelectronic-based devices.

2. Experimental

By using the sol-gel auto-combustion method, $NiFe_{2-x}Gd_xO_4$ ($x = 0.00$, 0.010, 0.15, 0.20 and 0.25) ferrite nanoparticles were synthesized [19–20]. As starting materials, analytical-grade ammonia, citric acid, ferric and gadolinium nitrates, and nickel nitrate were utilized. To create a clear solution, the starting materials were dissolved in deionized water in a stoichiometric ratio. Ni^{2+}, Gd^{3+}, and Fe^{3+} ions in the prepared aqueous solution were chelated by the addition of citric acid. The ratio of citric acid to the total moles of nitrate ions was adjusted to a molar ratio of 1 : 3. $P^H = 7$ was maintained by adding enough ammonia to the solution to neutralize it. After that, the neutralized solution was heated on a hot plate to roughly 100 °C while being constantly stirred. A viscous gel was seen a few hours later. The generated gel was ignited and burned entirely in a self-propagating combustion manner to form a loose powder, when the temperature was raised to 200 °C [21–22]. Then the powder was annealed for eight hours at 700 °C. Using a Phillips expert X-ray diffractometer, the XRD analysis of $NiFe_{2-x}Gd_xO_4$ ($x = 0.00$, 0.10, 0.15, 0.20 and 0.25), ferrite nanoparticles were estimated.

3. Results and Discussions

Figure 1 shows the XRD patterns of $NiFe_{2-x}Gd_xO_4$ ($x = 0.00$, 0.010, 0.15, 0.20 and 0.25) ferrite nanoparticles annealed at a temperature of 700 °C for 8 hours [23]. The XRD patterns show a single-phase cubic spinel structure. The XRD data revealed that the XRD peaks become narrower, while increasing Gd composition. With an increase in the Gd content, there is a small change in peak position, which could be caused by the different ionic radii of Gd (0.94 Å) and Fe (0.74 Å). The structural parameters like crystallite size and the lattice parameter were increased from 21.0288 to 27.04125 nm and 8.3325 to 8.3367 Å respectively with Gd^{+3} composition which can be attributed to the larger ionic radii of rare earth ions (Gd^{+3}) [23]. The x-ray density (ρ_x) was determined using the lattice parameter value and the following relation; the estimated values are given in Table 1

$$\rho_x = \frac{8M}{Na^3}, \text{ [21]} \tag{1}$$

where, M is known as the molecular weight of the composition, N is the Avogadro's number ($6.023 \times \times 10^{23}$ atoms/mole), and a is the lattice parameter.

The optical energy band gap (E_g) and refractive index (n) are the main parameters of the optical and electrical proficiencies of semiconducting materials. Typically, the semiconducting samples' optical energy band gap is determined by the photon absorption threshold. The optical properties of ferrites, such as their optical energy band gap, refractive index, absorption coefficient, extinction coefficient, and real and imaginary parts of their optical dielectric constant, can be explored through UV-visible absorption spectroscopy. These properties have significance for the utilization of ferrites in optical, optoelectrical, and photosensitive devices. The absorption spectra of the gadolinium-doped nickel ferrite $NiFe_{2-x}Gd_xO_4$ ($x = 0.00$, 0.010, 0.15, 0.20 and 0.25) nanoparticles calcinated at 700 °C were performed using UV-Vis spectrophotometer at 300 K in the wavelength range of 200–800 nm, and the typical absorbance peaks were seen between 250–300 nm [24]. Tauc plots, which are displayed in Fig. 2, *a–f*, were used to calculate the optical energy band gap using the following Kubelka–Munk equation [25]:

$$(\alpha h\nu)^{1/n} = A(h\nu - E_g), \tag{2}$$

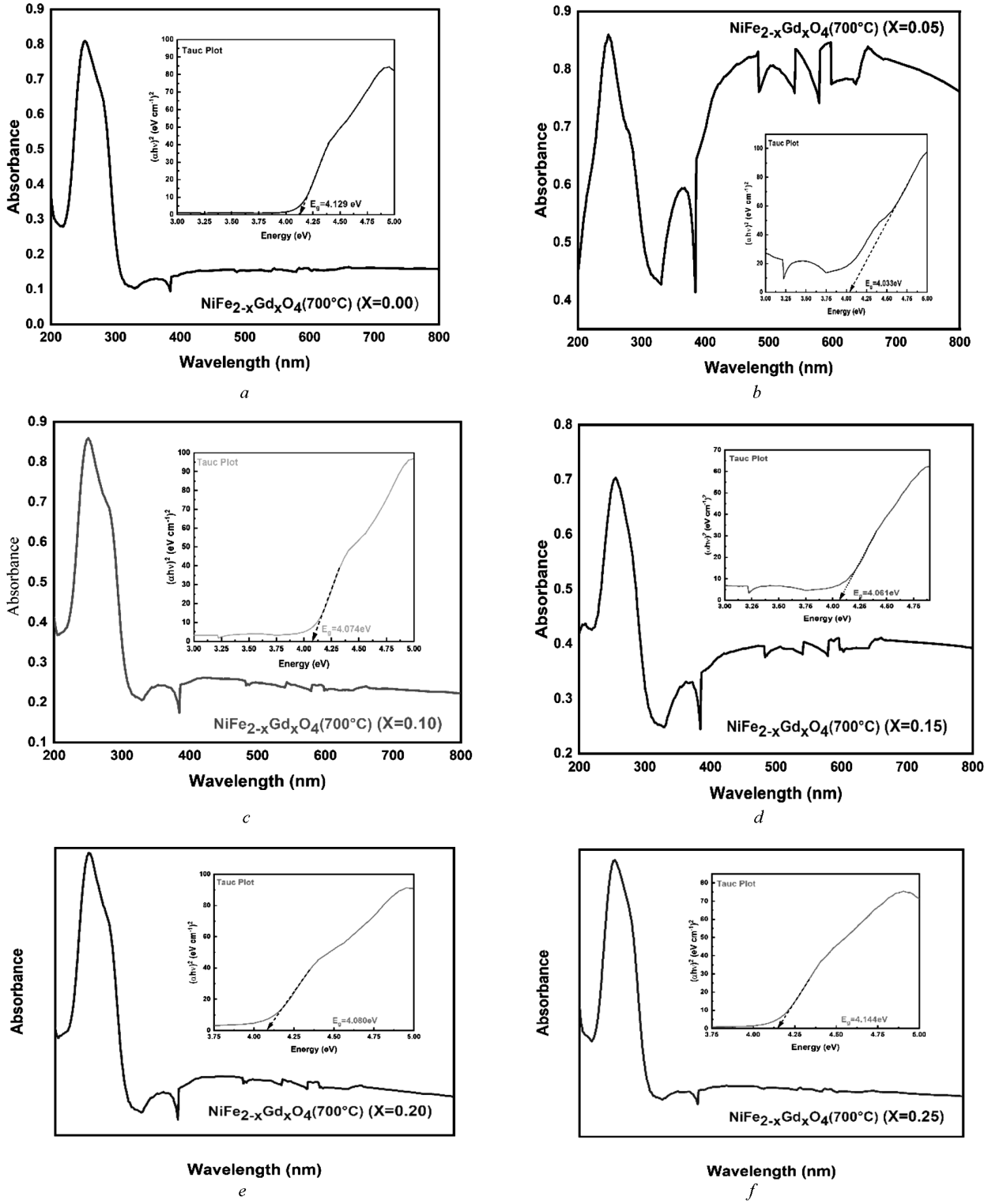

Fig. 2. Tauc plots of $NiFe_{2-x}Gd_xO_4$ ($x = 0.00, 0.05, 0.10, 0.15, 0.20\ 0.25$) nanoparticles calcinated at 700 °C

Table 1. **Lattice parameter (a), X-ray density(ρ_x), Optical energy band gap (E_g) from Tauc plot & x-ray density and Empirical relations Refractive indices (n) of $NiFe_{2-x}Gd_xO_4$ (x = 0.00, 0.05, 0.10, 0.15, 0.20 and 0.25) nanoparticles calcinated at 700 °C**

x	a (Å)	ρ_x (g/cm^3)	E_g (eV) (Tauc Plot)	E_g (eV) (X-ray density)	n (X-ray density)	n Moss [32]	n Ravindra *et al.* [33]	n Vandamme *et al.* [34]	n Reddy *et al.* [35]	n Anaei *et al.* [36]
0.00	8.3325	5.382	4.129	4.300	2.1140	2.1680	1.4180	2.0158	2.5011	2.5400
0.05	8.3326	5.497	4.033	4.170	2.1380	2.1847	1.4986	2.0417	2.5222	2.5660
0.10	8.3327	5.614	4.074	4.040	2.1620	2.2020	1.5792	2.0686	2.5442	2.5920
0.15	8.3329	5.730	4.061	3.917	2.1860	2.2191	1.6554	2.0951	2.5660	2.6166
0.20	8.3333	5.845	4.080	3.798	2.2100	2.2363	1.7292	2.1216	2.5879	2.6404
0.25	8.3367	5.954	4.144	3.690	2.2325	2.2525	1.7962	2.1465	2.6087	2.6620

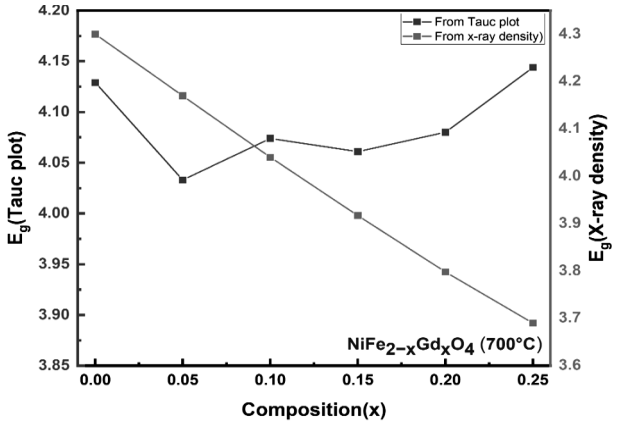

Fig. 3. Variation of optical band gap of $NiFe_{2-x}Gd_xO_4$ (x = = 0.00, 0.05, 0.10, 0.15, 0.20 0.25) nanoparticles calcinated at 700 °C with composition (obtained from Tauc plots and X-ray density)

where, α is known as absorption coefficient, h is the plank's constant, ν is the frequency, A is the absorbance, and n is related to electronic transitions. ($n = 2$ for direct allowed transitions; 3 for direct forbidden transitions; 3/2 for indirect forbidden transitions; 1/2 for indirect allowed transitions). To determine the probable transitions, the energy band gaps were observed extrapolating the straight portion from $(\alpha h\nu)^2$ vs $h\nu$ plots. The optical energy band gap values for all the samples were estimated, in the range of 4.033–4.144 eV and are furnished in Table 1. From XRD data, the optical energy band gap values for all the samples were estimated with the aid of X-ray density values in the range of 3.690–4.300 eV. It is evident that with increase of Gd composition, the optical energy band gap decreases (red-shift) which can be explained by the Burstein–Moss effect [26]. Similar to our findings, Hassouna, Dhaouad, *et al.* reported that, when Bi^{3+} was substituted for Ce^{3+} in $CePO_4$, the optical energy band gap decreased from 4.00 to 3.84 eV with composition and is known as a red-shift. The red shift is associated with the electronic transition from the dopant level to the conduction band or from the valence band to the dopant level [27]. Zinc aluminate was found to have a wider energy band gap (E_g = 4.11 eV) by Sampath *et al.* [28]. In order to find new linear and nonlinear optical materials for numerous possible applications, including integrated optical devices like switches, filters, modulators, *etc.*, it is crucial to evaluate the optical properties with account for the chemical composition of the material [27]. Figure 3 displays the optical energy band gaps for the samples derived from Tauc's plots and XRD data with different compositions. It is evidant that the optical energy band gaps estimated from Tauc plots are in good agreement with those calculated from the XRD data up to the composition, x = 0.15. Thereafter, the optical energy band gap values slightly deviate up to x = 0.25. The transparency to incident photons or radiation was measured by the refractive index.

The following relation was used to calculate the refractive index (n) using the X-ray density (ρ_x) [29]:

$$n^2 = 1 + 0.207\rho_x. \quad (3)$$

The estimated results are shown in Table 1. The composition, x = 0.25, had the maximum value of n (2.2325), while the composition, x = 0.00, had the minimum value of n (2.1140). It is clear that

n value increases with Gd composition. The variation of refractive index of $NiFe_{2-x}Gd_xO_4$ ($x = 0.00$, 0.010, 0.15, 0.20 and 0.25) nanoparticles calcinated at 700 °C with wavelength within the range of 200–800 nm is shown in Fig. 4. It is evident that, with the exception of composition, $x = 0.05$, the refractive indices for all the compositions increase gradually, reach the maximum, then decline in the range of 250–300 nm, and remain constant above 400 nm. The distinctive peaks were seen at the distinctive wavelengths, where the absorbance peaks were seen [24]. From the literature, we have several optical energy band gaps and refractive index relations in order to calculate the refractive index of a material. Some of the following empirical relations provided by various researchers are considered to measure the refractive index of a material [30–31]. We tried all these relations to our samples and did a comparative study

$$n^4 E_g = 95 \text{ eV [30]}, \tag{4}$$

$$n = 4.084 - 0.62E_g \text{ [31]}, \tag{5}$$

$$n^2 = 1 + \left(\frac{A}{\text{Eg} + B}\right)^2 \text{ [32]}. \tag{6}$$

Here, μ is the refractive index, $A = 13.6$ eV (hydrogen ionization energy), and $B = 3.47$ eV (constant which indicates the variation between the optical energy band gap and UV resonance energy).

$$n^4(E_g - 0.365) = 154 \text{ [33]}, \tag{7}$$

$$n = \frac{17 - E_g}{5} \text{ [34]}. \tag{8}$$

The obtained results are presented in Table 1. The refractive indices from the above empirical relations and X-ray density with composition are presented in Fig. 5. It is predicted that, for our samples, the Moss relation gives better results which would be in good concordance with values from the experiment. Similar to our study, Bardapurkar *et al.*, have calculated refractive index of lithium ferrite samples from the material density and also reported the comparative study with various empirical relations for calculations of refractive index of the material [35]. Liya Zhukova *et al.*, have determined the refractive index for $Ag_{1-x}Tl_xBr_{1-0.54x}I_{0.54x}$ crystals and scrutinized refractive index empirical calculations, with preferable Moss relation [25]. S.K. Tripathy examined a number of empirical formulas for calculating the refractive indices of various materials and forecasted more accurate results that would closely match experimental values in a medium with a wide interval of optical energy band gaps [36]. Additionally, each sample's velocity of light (V) has been estimated using the relation (9) below, and the outcomes of this calculation are listed in Table 2

$$V = \frac{3 \times 10^{10}}{n}. \tag{9}$$

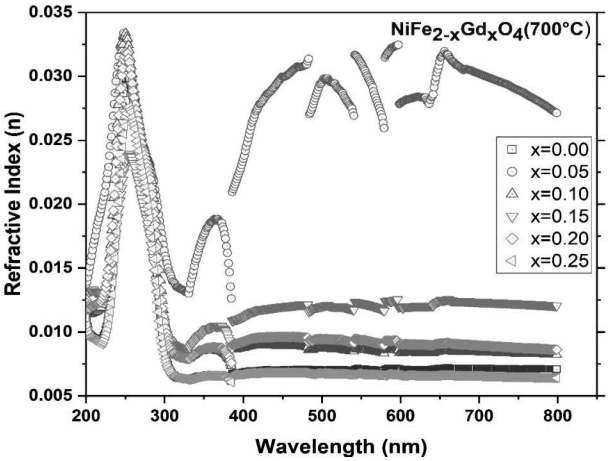

Fig. 4. Variation of refractive index of $NiFe_{2-x}Gd_xO_4$ ($x = 0.00$, 0.05, 0.10, 0.15, 0.20 0.25) nanoparticles calcinated at 700 °C with wavelength in UV-Visible region

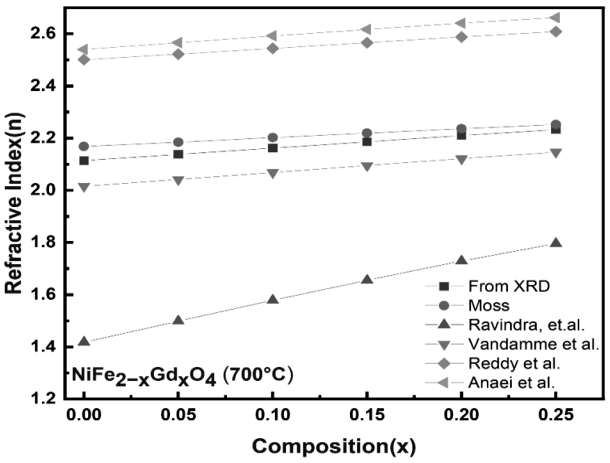

Fig. 5. Variation of refractive index of $NiFe_{2-x}Gd_xO_4$ ($x = 0.00$, 0.05, 0.10, 0.15, 0.20 0.25) nanoparticles calcinated at 700 °C with composition – various empirical relations

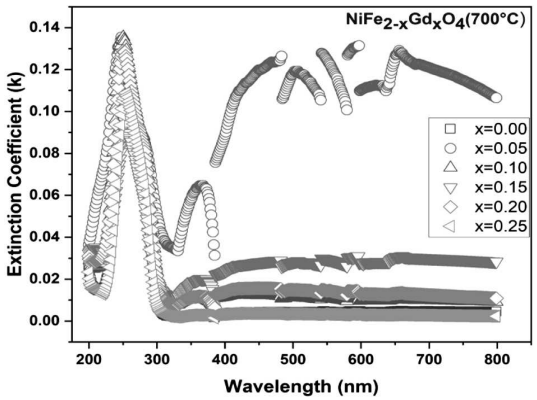

Fig. 6. Variation of extinction coefficient of $NiFe_{2-x}Gd_xO_4$ (x = 0.00, 0.05, 0.10, 0.15, 0.20 0.25) nanoparticles calcinated at 700 °C with wavelength in UV-Visible region

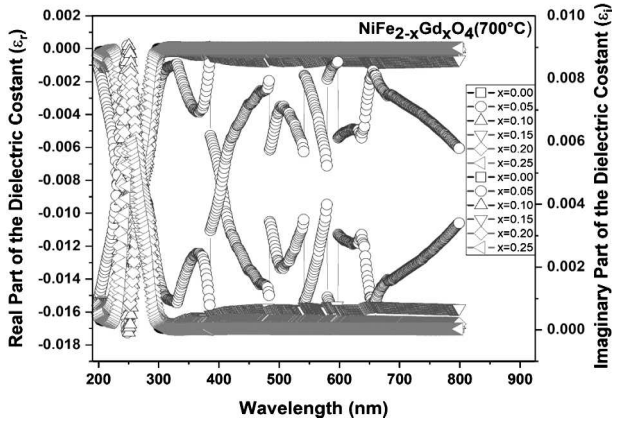

Fig. 7. Variation of real part and imaginary part of the dielectric constant of $NiFe_{2-x}Gd_xO_4$ (x = 0.00, 0.05, 0.10, 0.15, 0.20 0.25) nanoparticles calcinated at 700 °C with wavelength in UV-Visible region

Table 2. **Velocity of light through the sample (ν), reflectivity (R), absorption coefficient (α), transmission coefficient (T), optical dielectric constant (p) and dielectric susceptibility (χ), of $NiFe_{2-x}Gd_xO_4$ (x = 0.00, 0.05, 0.10, 0.15, 0.20 and 0.25) nanoparticles calcinated at 700 °C**

x	ν (cm/s) $\times 10^{10}$	R, %	α, cm^{-1}	T	p	χ
0.00	1.419	12.78	5.4380	0.7730	3.4690	0.2760
0.05	1.403	13.15	5.6138	0.7675	3.5710	0.2841
0.10	1.388	13.50	5.7894	0.7620	3.6742	0.2923
0.15	1.372	13.86	5.9647	0.7566	3.7786	0.3006
0.20	1.357	14.20	6.1396	0.7512	3.8841	0.3090
0.25	1.344	14.54	6.3032	0.7461	3.9840	0.3170

The composition, $x = 0.00$, had the maximum value (1.419 cm/s), while the composition, $x = 0.25$, had minimum value (1.34 cm/s). It is clear evident that the velocity of light decreases with Gd composition. The following refractive index relation was used to calculate the reflection coefficient, also known as reflectivity (R) [37, 38]:

$$R = \left(\frac{n-1}{n+1}\right)^2 \times 100\%. \tag{10}$$

Estimated R values are presented in Table 2. The composition, $x = 0.25$, had maximum value of R (14.54%), while the composition, $x = 0.00$ had minimum value of R (12.78%). It is evident that reflectivity increases with Gd composition. The Kubelka–Munk function $F(R)$ can be used to determine the absorption coefficient (α) [39]:

$$\alpha = \frac{(1-R)^2}{2R}. \tag{11}$$

The obtained α values are given in Table 2. The composition, $x = 0.25$, had maximum value of α (6.3033 cm^{-1}), while the composition, $x = 0.00$ had minimum value of α (5.4380 cm^{-1}). It is evident that α value increases with Gd composition.

The following relation can be employed to calculate the extinction coefficient

$$k = \frac{\alpha\lambda}{4\pi}, \tag{12}$$

where, k is the extinction coefficient, λ is the wavelength, and α is the absorption coefficient. The variation of the extinction coefficient for $NiFe_{2-x}Gd_xO_4$ (x = 0.00, 0.010, 0.15, 0.20, and 0.25) nanoparticles calcined at 700 °C and with a wavelength range of 200–800 nm is displayed in Fig. 6. With the exception of composition, $x = 0.05$, it is evident that the extinction coefficient of all the samples increases gradually, reaches its maximum, and then declines in the 250–300 nm wavelength inyrtval. After 400 nm, the extinction coefficient remained constant. The transmission coefficient (T) serves as a measure for the amount of electromagnetic radiation that can flow through the specified sample. The following relation can be used to calculate it [40]:

$$T = \frac{2n}{n^2+1}. \tag{13}$$

Table 2 provides the estimated T values. The composition, $x = 0.00$, had maximum value of $T(0.7730)$, while the composition, $x = 0.25$, had minimum value of $T(0.7461)$. It is evident that transmission coefficient decreases with Gd composition. A material's optical and dielectric characteristics can be correlated to generate an optical dielectric constant (p), which is necessary for the creation of functional devices for potential uses. The dielectric constant exhibits a strong dependence on the photon energy due to interactions between moving electrons and photons. This can be explained by the material's ease of electromagnetic wave transmission. The relationship between the refractive index (n) and optical dielectric constant (p) is as follows [41]:

$$p = n^2 - 1. \tag{14}$$

Table 2 provides estimated p values. The composition, $x = 0.25$, had maximum value of p (3.9840), while the composition, $x = 0.00$, had minimum value of p (3.4690). It is evident that p value increases with Gd composition. Figure 7 illustrates the variation of the real and imaginary parts of the dielectric constant of $NiFe_{2-x}Gd_xO_4$ (x = 0.00, 0.010, 0.15, 0.20, & 0.25) nanoparticles that were calcined at 700 °C and with a wavelength range of 200–800 nm. It is evident that, with the exception of Gd composition, $x = 0.05$, the real and imaginary parts of the dielectric constant of all the compositions reach their maximum and then decline in the wavelength region of 250–300 nm. Beyond 400 nm, the dielectric constant remained constant. A quantitative indicator of the sample's ability to be momentarily polarized in response to an external field is its susceptibility. χ is a more convenient term to describe the physical interaction of electromagnetic waves with matter than the refractive index, because it is zero in a vacuum. The degree of polarization and refractive index are directly correlated, as demonstrated by the relationship above. Secondary wave sources are produced by the interaction between electrons and electromagnetic waves. The properties such as absorption, dispersion, polarization, amount of incident electromagnetic energy transferred to the vibronic energy of the material, *etc.* are modified by the phase difference between any two sources. Refractive index may be utilized as well to calculate the dielectric/electric susceptibility (χ) using the following relation [42]:

$$\chi = \frac{n^2 - 1}{4\pi}. \tag{15}$$

Table 2 provides the estimated χ values. The composition, $x = 0.25$, had maximum value (0.3170), while the composition, $x = 0.00$, had minimum value of χ (0.2760). It is evident that χ value increases with Gd composition. There exists a significant correlation between the optical energy band gap and refractive index, which determines all the above optical parameters. Optimizing the synthesis technique and selecting suitable doping can control the ideal values of these optical parameters to meet the needs of particular applications.

4. Conclusion

The XRD confirmed the cubic spinel structure. In all the prepared samples, the typical absorbance peak was observed in the UV region. The optical energy band gaps were found in the range of 4.033–4.144 eV calculated by Tauc plots and 3.69–4.300 eV calculated by X-ray density. They appear in good agreement with each other. The refractive index calculated using the X-ray density was observed in very good agreement with the Moss relation. The influence of the Gd composition was clearly observed in the fine tuning of the optical energy band gap, and we have found Gd impact on all the optical parameters such as reflectivity, absorption coefficient, extinction coefficient, transmission coefficient, optical dielectric constant, and dielectric susceptibility.

1. L. Jaswala, B Singh. Ferrite materials: A chronological review. *J. Integr. Sci. Technol.* **2**, 69 (2014).
2. S. Yadav. Development of a low loss Mn–Zn Ferrite Material for power applications. (2006).
3. G. Rana, P. Dhiman, A. Kumar, D.V.N. Vo, G. Sharma, S. Sharma, M. Naushad. Recent advances on nickel nanoferrite: A review on processing techniques, properties and diverse applications. *Chem. Eng. Res. Des.* **175,** 182 (2021).
4. W.A. Khoso, N. Haleem, M.A. Baig, Y. Jamal. Synthesis, characterization and heavy metal removal efficiency of nickel ferrite nanoparticles (NFN's). *Sci. Rep.* **11** (1), 1 (2021).
5. G.N. Rajivgandhi, G. Ramachandran, C.C. Kanisha, N.S. Alharbi, S. Kadaikunnan, J.M. Khaled, K.F. Alanzi, W.J. Li. Effect of Ti and Cu doping on the structural, optical, morphological and anti-bacterial properties of nickel ferrite nanoparticles. *Results Phys.* **23,** 104065 (2021).

6. J. Hwang, M. Choi, H.-S. Shin, B.-K. Ju, M. Chun. Structural and magnetic properties of NiZn ferrite nanoparticles synthesized by a thermal decomposition method. *Appl. Sci.* **10** (18), 6279 (2020).
7. B. Hussain. *Synthesis, Characterization and Antibacterial Study of Silver Doped Manganese Ferrite Nanocomposites.* MS & PhD Thesis (2021).
8. H. Du, O.U. Akakuru, C. Yao, F. Yang, A. Wu. Transition metal ion-doped ferrites nanoparticles for bioimaging and cancer therapy, *Transl. oncol.* **15** (1), 101264 (2022).
9. S. Naik, A. Salker. Change in the magnetostructural properties of rare earth doped cobalt ferrites relative to the magnetic anisotropy. *J. Mater. Chem.* **22** (6), 2740 (2012).
10. R.J. Elliott. *Magnetic Properties of Rare Earth Metals* (Springer, 2013).
11. R. Moon, W. Koehler, J. Cable, H. Child. Distribution of magnetic moment in metallic Gadolinium. *Phys. Rev. B* **5**, 997 (1972).
12. F. Cheng, C. Liao, J. Kuang, Z.Xu, C. Yan, L. Chen, H. Zhao, Z. Liu. Nanostructure magneto-optical thin films of rare earth (RE = Gd, Tb, Dy) doped cobalt spinel by sol–gel synthesis. *J. Appl. Phys.* **85**, 2782 (1999).
13. S. Mahalakshmi, K. Srinivasa Manja, S. Nithiyanantham. Electrical properties of nanophase ferrites doped with rare earth ions. *J. Supercond. Nov. Magn.* **27**, 2083 (2014).
14. M.S.S. Adam, A.M. Hafez, M.M. Khalaf. Rare earth Ce- and Nd-doped spinel nickel ferrites as effective heterogeneous catalysts in the (ep) oxidation of alkenes. *J. Iran. Chem. Soc.* **17** (12), 3237 (2020).
15. C.S. Pawar, M.P. Gujar, V.L. Mathe. Optical properties of spin-deposited nanocrystalline Ni–Zn ferrite thin films processed by sol–gel. *J. Supercond. Nov. Magn.* **30,** 615 (2017).
16. V. Dimitrov, T. Komatsu. An interpretation of optical properties of oxides and oxide glasses in terms of the electronic ion polarizability and average single bond strength, *J. Univ. Chem. Technol. Met.* **45**, 219 (2010).
17. M.K. Halimah, M.F. Faznny, M.N. Azlan, H.A.A. Sidek. Optical basicity and electronic polarizability of zinc borotellurite glass doped La^{3+} ions. *Results Phys.* **7**, 581 (2017).
18. G. Rana, P. Dhiman, A. Kumar, D.V.N. Vo, G. Sharma, S. Sharma, M. Naushad. Recent advances on nickel nanoferrite: A review on processing techniques, properties and diverse applications. *Chem. Eng. Res. Des.* **175** (12), 182 (2021).
19. K. Rama Krishn, K. Vijaya Kumar, D. Ravinder. Structural and electrical conductivity studies in nickel-zinc ferrite. *Adv. Mater. Phys. Chem.* **2**, 185 (2012).
20. K.V. Kumar, S.D. Bhavani. Influence of calcination temperature on physical and optical properties of nickel chromite nanoparticles. *Science of Sintering* **54** (4), 457 (2022).
21. K.V. Kumar, S.D. Bhavani. Impact of calcination temperature on structural and optical properties of erbium-doped zinc ferrite nanoparticles. *Phase Transitions* **95** (11), 770 (2022).
22. Sara Durga Bhavani, K. Vijaya Kumar. Effect of calcination temperature on structural and optical properties of nickel aluminate nanoparticles. *East Eur. J. Phys.* **3**, 355 (2023).
23. Sara Durga Bhavani, A.T. Raghavender, K. Vijaya Kumar, B. Purna Chandra Rao. Effect of annealing temperature on the XRD and IR properties of Gd doped nickel ferrites nanoparticles. *Eur. Chem. Bull.* **12** (4), 10479 (2023).
24. K.V. Kumar. Tunable optical bandgap of gadolinium substituted nickel-zinc ferrite nanoparticles, effect of calcination temperature on its optical parameters. *Adv. in Mater. Phys. Chem.* **12**, 33 (2022).
25. A. Korsakov, D. Salimgareev, A. Lvov, L. Zhukova. IR spectroscopic determination of the refractive index of $Ag_{1-x}Tl_xBr_{1-0.54x}I_{0.54x}$ ($0 \leq x \leq 0.05$) crystals. *Opt. Laser Technol.* **93**, 18 (2017).
26. B. Joseph, P.K. Manoj, V.K. Vaidyan. Studies on the structural, electrical and optical properties of Al-doped ZnO thin films prepared by chemical spray deposition. *Ceram. Int.* **32**, 487 (2006).
27. A. Fadhalaoui, S. Kouass, H. Dhaouad. $Bi_xCe_{1-x}PO_4$ (x = 0.00, 0.02, and 0.08) nanorods: Structural, electrical, optical, and electrochemical properties. *Ionics* **24**, 429 (2018).
28. K. Sampath, D.G. Kanhere, R. Pandey. Electronic structure of spinel oxides: Zinc aluminate and zinc gallate. *J. Phys. Condens. Matter.* **11**, 3635 (1999).
29. O.L. Anderson, E. Schreiber. The relation between refractive index and density of minerals related to the Earth's mantle. *J. Geophys. Res.* **70** (6), 1463 (1965).
30. T.S. Moss. Relation between the refractive index and energy gap of semiconductors. *Phys. Status Solidi B* **131**, 415 (1985).
31. V.P. Gupta, N.M. Ravindra. Comments on the moss formula. *Phys. Status Solidi (b)* **100** (2), 715 (1980).
32. P. Herve, L.K.J. Vandamme. General relation between refractive index and energy gap in semiconductors. *Infrared Phys. Technol.* **35** (4), 609 (1994).
33. R.R. Reddy, Y.N. Ahammed, K.R. Gopal, P.A. Azeem, T.V.R. Rao, P.M. Reddy. Optical electronegativity, bulk modulus and electronic polarizability of materials. *Opt. Mater.* **14**, 355 (2000).
34. M. Anani, C. Mathieu, S. Lebid, Y. Amar, Z. Chama, H. Abid. Model for calculating the refractive index of a III–V semiconductor. *Comput. Mater. Sci.* **41**, 570 (2008).
35. N.P. Barde, V.R. Rathod, P.S. Solanki, N.A. Shah, P.P. Bardapurkar. On the structural, refractive index and energy bandgap based optical properties of lithium ferrite nanoparticles dispersed in silica matrix. *Appl. Surf. Sci. Adv.* **11**, 100302 (2022).
36. S.K. Tripathy. Refractive indices of semiconductors from energy gaps. *Opt. Mater.* **46**, 240 (2015).
37. Z. Serbetçi, H.M. Nasser, Yaku Phanoglu. Photoluminescence and refractive index dispersion properties of ZnO nanofibers grown by sol-gel method. *Spectrochim. Acta, Part A* **86**, 405 (2012).

38. K.B. Modi, S.J. Shah, N.B. Pujara, T.K. Pathak, N.H. Vasoya, I.G. Jhala. Infrared spectral evolution, elastic, optical and thermodynamic properties study on mechanically milled $Ni_{0.5}Zn_{0.5}Fe_2O_4$ spinel ferrite. *J. Mol. Struct.* **1049**, 250 (2013).
39. K.B. Modi, P.Y. Raval, P.R. Pansara, I.R. Badi, D.R. Devmurari, S.S. Munshi, P.U. Sharma. On the relationship between structural-optical parameters of $Y_{3-x}Fe_{5+x}O_{12}$ garnet ferrites and the oxide additivity rule. *J. Supercond. Nov. Magn.* **29**, 1931 (2016).
40. R.D. Shannon, R.X. Fischer. Empirical electronic polarizabilities in oxides, hydroxides, oxyfluorides, and oxychlorides. *Phys. Rev. B Condens. Matter Mater. Phys.* **73**, 235111 (2006).
41. B. Bhatia, S.L. Meena, V. Parihar, M. Poonia. Optical basicity and polarizability of Nd^{4+}-doped bismuth borate glasses. *New J. Glass. Ceram.* **05**, 44 (2015).
42. S.A. Umar, M.K. Halimah, K.T. Chan, A.A. Latif. Polarizability, optical basicity and electric susceptibility of Er^{3+} doped silicate borotellurite glasses. *J. Non Cryst. Solids* **471**, 101 (2017).

Received 29.12.23

С. Дурга Бхавані, К. Віджая Кумар,
Б. Пурна Чадра Рао, Ч. Шілпа Чакра,
Кіран Кумар Ганта

ДОСЛІДЖЕННЯ ТОНКОГО НАЛАШТУВАННЯ ОПТИЧНОЇ ЗАБОРОНЕНОЇ ЗОНИ І РІЗНИХ ОПТИЧНИХ ПАРАМЕТРІВ ЗМІНОЮ ВМІСТУ ГАДОЛІНІЮ В NGFO ФЕРИТОВИХ НАНОЧАСТИНКАХ

За допомогою золь-гель методу автоспалення отримано наночастинки фериту з нікелем і гадолінієм, що має склад $NiFe_{2-x}Gd_xO_4$ ($X = 0,00$, 0,05, 0,10, 0,15, 0,20, та 0,25), і кальциновано зразки при 700°. Рентґенограми свідчать про формування фази зі структурою шпінелі. Для всіх зразків спостерігається пік поглинання біля 250–300 нм. Використовуючи діаграми Таука і дані рентґеноструктурного аналізу, ми знайшли, що ширина оптичної забороненої зони дорівнює, відповідно, 4,033-4,144 еВ та 3,69–4,3 еВ. Знайдено, що цей та інші оптичні параметри залежать від вмісту гадолінію.

Ключові слова: NGFO наночастинки, оптична заборонена зона, показник заломлення, коефіцієнт поглинання, втрати при відбитті, оптична діелектрична константа.